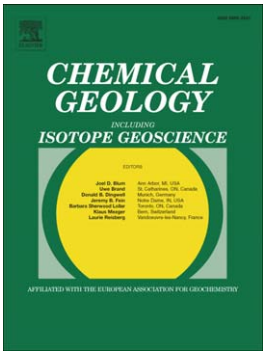

Accepted Manuscript

The controls of post-entrapment diffusion on the solubility of chalcopyrite daughter crystals in natural quartz-hosted fluid inclusions

Edward T. Spencer, Jamie J. Wilkinson, John Nolan, Andrew J. Berry

PII: S0009-2541(15)00324-1
DOI: doi: 10.1016/j.chemgeo.2015.07.005
Reference: CHEMGE 17632

To appear in: *Chemical Geology*

Received date: 17 March 2015
Revised date: 1 July 2015
Accepted date: 2 July 2015

Please cite this article as: Spencer, Edward T., Wilkinson, Jamie J., Nolan, John, Berry, Andrew J., The controls of post-entrapment diffusion on the solubility of chalcopyrite daughter crystals in natural quartz-hosted fluid inclusions, *Chemical Geology* (2015), doi: 10.1016/j.chemgeo.2015.07.005

The controls of post-entrapment diffusion on the solubility of chalcopyrite daughter crystals in natural quartz-hosted fluid inclusions

Edward T. Spencer[1,2], Jamie J. Wilkinson[1,2], John Nolan[1] and Andrew J. Berry[1,2,3]

[1] *Department of Earth Science and Engineering, Imperial College London, United Kingdom, SW7 2AZ*
[2] *Earth Sciences Department, Natural History Museum, London, United Kingdom, SW7 5BD*
[3] *Research School of Earth Sciences, Australian National University, Canberra, 2601, Australia*

Corresponding Author email: es406@imperial.ac.uk
Corresponding Author telephone: +44 (0)7805568061

Abstract

The presence of chalcopyrite daughter crystals in natural quartz-hosted fluid inclusions that do not dissolve when heated to trapping conditions suggests that inclusions are subject to post-entrapment modifications that affect chalcopyrite solubility. Previous double capsule experiments conducted by Mavrogenes and Bodnar (1994) concluded that the post-entrapment outward diffusion of H_2 is responsible for the presence of non-dissolvable chalcopyrite crystals in natural, quartz-hosted brine inclusions. However, recent studies have shown that quartz-hosted inclusions can also be modified by diffusional H^+ loss and Cu^+ gain. This means that multiple factors may influence chalcopyrite solubility in different fluid inclusion types. In this study, the experimental procedure of Mavrogenes and Bodnar (1994) was recreated in order to rehydrogenate quartz-hosted, chalcopyrite-bearing fluid inclusions from the El Teniente Cu-Mo porphyry deposit, Chile. These inclusions had a range of salinities and densities. Results show that the experimental technique is successful for fluid inclusions that contain relatively small chalcopyrite daughter crystals and have moderate salinities (>5 wt.% $NaCl_{eq}$). In contrast, chalcopyrite crystals do not dissolve in low density vapor inclusions even after rehydrogenation. The failure of chalcopyrite crystals to dissolve in these inclusions is attributed to their lower initial pH and higher sulfide concentrations, which led to greater post-entrapment H^+ loss and Cu^+ gain. This considered, Cu concentrations in moderate to high salinity inclusions are likely to reflect those present at trapping, suggesting that H_2 loss is the primary control on the failed dissolution of chalcopyrite. By contrast, Cu concentrations in S-rich vapor inclusions can increase considerably via inward Cu^+ diffusion in the presence of an external Cu-bearing fluid and a pH gradient between the inclusion and this fluid (Lerchbaumer and Audétat, 2012; Seo and Heinrich, 2013). In accordance with these studies, the post-entrapment modification of Cu concentrations in vapor inclusions may undermine the apparent importance of phase separated vapors as a key agent of Cu transport and deposition in porphyry systems.

1. Introduction

Fluid inclusion analysis is a fundamental technique for determining the physical and chemical characteristics of fluids that were once present in geological environments. One of the assumptions of this approach is that the concentration of elements within a fluid inclusion remains unchanged following entrapment in a host mineral such as quartz. Despite this, it has been suggested that hydrogen diffusion (H_2) through quartz can occur, resulting in significant changes in inclusion redox potentials (e.g. Roedder, 1984). This is supported by spectrophotometric diffusion tests in the temperature range 400-900°C, which showed that over time hydrogen can migrate through quartz via bulk diffusion (Kats *et al*., 1962). Changes in inclusion fH_2 have subsequently been used to explain the presence of anomalous daughter phases, volatile species and isotopic ratios in natural quartz-hosted fluid inclusions (Hall, 1989; Hall and Bodnar, 1990; Hall *et al*., 1991; Morgan *et al*., 1993; Mavrogenes and Bodnar, 1994).

The effect of hydrogen diffusion on metal-sulfide solubility, in particular the impact on sulfide daughter minerals, was studied previously using small, chalcopyrite-bearing, high salinity (~55 wt.% $NaCl_{eq}$) fluid inclusions from the Red Mountain porphyry Cu deposit, Arizona (Mavrogenes and Bodnar, 1994). Here, the occurrence of large numbers of coeval, chalcopyrite-bearing fluid inclusions with broadly uniform vapor fractions, number of phases and volumetric proportions provided strong evidence that the chalcopyrite crystals were daughter crystals and not accidentally incorporated grains. The high Cu concentrations of these inclusions were interpreted to be typical of the high solubility of Cu in saline magmatic-hydrothermal fluids and were in accordance with solubility data obtained from synthetic fluid inclusion studies (Mavrogenes *at al.*, 1992). However, these apparent daughter crystals did not dissolve, as they should do, when heated above the inferred trapping temperatures but did dissolve once the samples had been equilibrated in double-capsule experiments designed to diffuse hydrogen into the trapped fluids. These results are consistent with post-entrapment loss of hydrogen as H_2 from the fluid inclusions by diffusion through quartz and imply that fH_2 is a key control on the solubility of chalcopyrite in porphyry brines.

Chalcopyrite daughter crystals have also been reported in a wide range of other fluid inclusion types from porphyry systems, including low salinity liquid, intermediate density and vapor inclusions (e.g. Vry, 2010). The high Cu concentrations in these inclusions are

inconsistent with experimental data (e.g. Candela and Holland, 1984, 1986; Hemley *et al*., 1992; Bai and Koster van Groos, 1999; Archibald *et al*. 2002; Hack and Mavrogenes, 2006; Simon *et al*., 2006) and it has recently been shown that these high concentrations may be due to a different post-entrapment modification involving diffusion through quartz of small, univalent ions such as H^+, Cu^+, Na^+, Li^+ and Ag^+ in the presence of an external fluid (Li *et al*., 2009; Zajacz *et al*., 2009; Lerchbaumer and Audétat, 2012).

Reequilibration experiments of synthesized coexisting vapor and brine inclusions in quartz showed that Cu^+ diffusion can significantly modify the Cu concentrations of fluid inclusions (Lerchbaumer and Audétat, 2012). Sulfur is interpreted to enhance the inward migration of Cu via the precipitation of Cu-sulfide crystals such as $CuFeS_2$ by the reaction of incoming Cu^+ with trapped H_2S and/or SO_2. Substantial Cu-gain only occurred when the external fluids were less acidic than the inclusion fluid suggesting that outward diffusion of H^+ was responsible for maintaining charge balance. This process was interpreted to continue until the system reached chemical equilibrium, explaining why S-rich vapor inclusions appear to be particularly prone to Cu gain (Lerchbaumer and Audétat, 2012) and why quartz-hosted inclusions commonly record 1:2 molar ratios of Cu and S (i.e. buffered to chalcopyrite stoichiometry by adding Cu until S content of the inclusion was exhausted; Seo *et al*., 2009). A study of coeval fluid inclusions hosted by topaz and quartz showed that the average Cu concentrations in S-rich vapor inclusions tended to be lower in topaz than in the same fluid populations hosted in the quartz (Seo and Heinrich, 2013). This was attributed to the smaller diffusion channels in topaz, which prevented Cu^+ diffusion into the vapor inclusions. By contrast, Cu concentrations in coeval brine inclusions are similar in both host minerals, leading to the conclusion that brine inclusions are subject to much lower degrees of H^+ loss and Cu^+ gain, presumably due to a lower reduced S content (Seo and Heinrich, 2013).

Given these results, it is now unclear whether outward H_2 diffusion affecting fO_2, inward Cu diffusion, or changes in pH via H^+ diffusion is the main control on the non-dissolution of chalcopyrite daughter minerals in porphyry-related fluid inclusions. We might predict that chalcopyrite daughters in brine inclusions may dissolve on heating after rehydrogention if it is only diffusive H_2 loss that has occurred. By contrast, low salinity inclusions may have undergone significant diffusive Cu gain meaning that rehydrogenation alone would not be expected to lead to chalcopyrite redissolution.

The present study uses the experimental technique of Mavrogenes and Bodnar (1994) to rehydrogenate quartz-hosted fluid inclusions with variable salinities from the El Teniente Cu-Mo porphyry deposit, Chile. This deposit was selected due to the abundance of chalcopyrite daughter crystals hosted in both intermediate density aqueous and low salinity vapor inclusions. In addition, fluid inclusion compositions from this deposit have been previously studied previously using LA-ICP-MS (Klemm *et al*., 2007; Vry, 2010) so that there is extensive knowledge of fluid inclusion compositions that was not available in the study of Mavrogenes and Bodnar (1994). This allows for a more quantitative assessment of the reactions that govern chalcopyrite solubility before and after rehydrogenation. Unlike in the study of Mavrogenes and Bodnar (1994), the same inclusions were measured before and after each experiment to confirm that chalcopyrite dissolution (if it occurred) was a function of increased fH_2 and that the inclusions studied were not subject to leakage or volume changes during the experiments. In addition, this allowed inclusions at variable depths in the sample to be examined in order to test for any limits of H_2 diffusion into the samples.

2. Samples

The El Teniente supergiant Cu-Mo porphyry deposit is located on the western margin of the Andean Cordillera, within the confines of the central Chilean porphyry copper belt. The deposit is one of the world's largest repositories of Cu with a current and mined resource total in excess of 94.4 Mt (Cannell *et al.,* 2005). Main mineralization type quartz ± anhydrite veins (type 6a, type 6b and type 8 veins; Vry *et al*., 2010) usually contain multiple generations of fluids trapped in inclusions with typical diameters of 5-40 µm. Previous microthermometric and LA-ICP-MS analyses revealed that they have highly variable densities (0.25-1.5 g/cm^3), salinities (0.1-60 wt.% $NaCl_{eq}$) and Cu concentrations (100-25,000 ppm (Vry, 2010). Chalcopyrite daughter minerals are common in the more Cu-rich inclusions and pyrite and molybdenite have also been observed (Klemm *et al.*, 2007; Vry, 2010).

Fluid inclusion types at El Teniente are subdivided into salt-undersaturated (type A) inclusions and salt-oversaturated (type B) inclusions based on the presence or absence of a halite daughter crystal at room temperature (Vry, 2010). A total of nine fluid inclusion types have been recognized (Fig. 1), five of which contain opaque daughter phases. The most abundant of these are 1-3 µm, triangular, chalcopyrite daughter crystals, particularly in intermediate salinity A_{IDO} and A_{LO} inclusions and high salinity B_{HO} brine inclusions. The presence of opaque-bearing inclusions in assemblages that have consistent microthermometric properties, compositions and number of phases supports the interpretation that these opaques are daughter phases and not accidentally trapped crystals. Chalcopyrite daughters are also reported in rare, multiphase B_M inclusions and A_{VO} inclusions (Vry, 2010).

As with the inclusions from Red Mountain, Arizona (Mavrogenes and Bodnar, 1994), the chalcopyrite daughter crystals in all inclusion types from El Teniente failed to dissolve when heated. This contrasts with the successful dissolution of chalcopyrite daughter crystals in synthetic fluid inclusions (e.g. Sterner and Bodnar, 1984) that have similar compositions and microthermometric properties to those encountered in porphyry Cu systems. One possible explanation for this is that the opaque-bearing, quartz-hosted inclusions at El Teniente have been subject to post-entrapment modification.

Type	Fluid inclusion characteristics
A_L	Vf = 0-40%
A_{LO}	Vf = 0-40% + opaque daughter
A_{ID}	Vf = 40-60%
A_{IDO}	Vf = 40-70% + opaque daughter
A_V	Vf = 60-90%
A_{VO}	Vf = >70% + opaque daughter
B_H	Vf = ~20% + halite daughter
B_{HO}	Vf = ~20% + halite + opaque
B_M	Vf = ~20% + multiple daughters

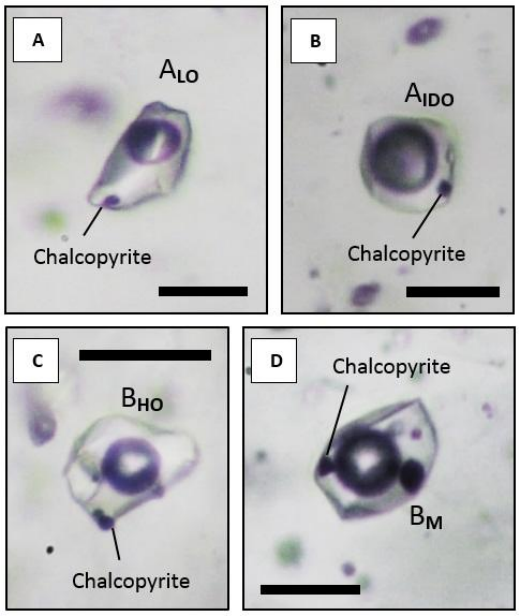

Fig. 1: Table of fluid inclusion types observed at El Teniente (adapted from Vry, 2010). Type A inclusions = aqueous fluid inclusion types with variable vapor fractions and daughter phases. Type B inclusions = brine inclusions classified based on contained daughter phases. Vf = volumetric proportion of vapor at room temperature. L = liquid, LO = liquid +opaque, ID = intermediate density, IDO = intermediate density +opaque, V = vapor, VO = vapor +opaque, H = halite, HO = halite+opaque, M = multisolid. (A-D) = photomicrographs of different fluid inclusion types that contain chalcopyrite daughter crystals. (A) an A_{LO} inclusion; (B) an A_{IDO} inclusion (C) a B_{HO} inclusion with a small chalcopyrite daughter crystal; (D) a B_M inclusion with 3 opaque daughter crystals. Scale bars = 10 µm.

3. Methodology

3.1 Fluid Inclusion Microthermometry

Two quartz vein samples were selected for analysis (08-2452-577 and 07-2406-07) based on their coarse textures, lack of anhydrite and abundance of chalcopyrite-bearing fluid inclusions with a range of densities and salinities. Both samples were associated with deep zones of Cu-Mo mineralization related to separate diorite finger porphyries on the eastern side of the deposit. These were prepared as double-polished sections with thicknesses of ~600 µm and broken into several pieces of 1-3 mm length and 2 mm width so that they could fit inside the 3 mm internal diameter (ID) Pt capsules used in the rehydrogenation experiments.

Microthermometry was carried out using a Linkam MDS600 heating-freezing stage with operating temperatures between -190°C and 600°C and heating/cooling rates of 0.1–99°C/min. Quartz wafers were optically imaged using a motorized stage to produce a grid of high-resolution images. This allowed the position of each chalcopyrite-bearing inclusion to be

recorded so that they could be relocated after rehydrogenation experiments. Each inclusion was classified in accordance with Vry (2010; Fig. 1) and the inclusion dimensions and vapor fractions (*Vf*) were recorded. Rounded to sub-rounded fluid inclusions were studied in order to reduce the chance of decrepitation during microthermometry and rehydrogenation. All inclusions studied were located within 50 μm of the sample surface in order to be within the likely range of hydrogen diffusion during the rehydrogenation experiments (c.f. Kats *et al*., 1962; Mavrogenes and Bodnar, 1994).

Freezing tests were completed first by cooling samples to approximately -110°C and then heating at rates of 30°C to 0.1°C/min. All phase transition temperatures were recorded during heating cycles with heating rates of ≤1°C/min, which resulted in a precision of ±0.1°C. Accuracy, based on measurement of in-house synthetic fluid inclusion standards, is ±0.1°C from -100 to +30°C and ±0.4°C at higher temperatures. The temperature of final ice melting (Tm_{ice}) was recorded in order to determine the salinity of salt-undersaturated inclusions, reported as wt.% $NaCl_{eq}$ (Bodnar, 1993; Bodnar and Vityk, 1994). Samples were heated to a maximum temperature of 590°C under constant observation to check whether chalcopyrite daughter crystals dissolved and, if so, at what temperature. Liquid-vapor homogenization (Th) and halite dissolution temperatures (Tm_{Halite}) were recorded as well as the mode of total homogenization: $Th_{L+V\rightarrow L}$, $Th_{L+V\rightarrow V}$, $Th_{L+V+S\rightarrow L+V\rightarrow L}$ or $Th_{L+V+S\rightarrow L+S\rightarrow L}$. Where brine inclusions homogenized by vapor disappearance, fluid inclusion salinity, density and minimum trapping pressure were obtained by using existing experimental (Bodnar and Sterner, 1985; Sterner *et al*., 1988; Bodnar, 1992) and theoretical (Bischoff and Pitzer, 1989; Anderko and Pitzer, 1993) data for the vapor-saturated halite solubility curve and liquid-vapor surfaces in the H_2O-NaCl system (c.f. Becker *et al*., 2008). For brine inclusions that homogenized by halite dissolution, minimum trapping pressures and salinities were interpreted based on experimental data (Bodnar, 1994; Bodnar and Vityk, 1994; Becker *et al*., 2008) and the relationship between Tm_{Halite} and $Th_{L\text{-}V}$ for a solution of 40 wt.% $NaCl_{eq}$ as derived by Becker *et al*. (2008).

3.2 Rehydrogenation Experiments

Eighty-seven fluid inclusions were analyzed by microthermometry. These displayed total homogenization temperatures between 350°C and >590°C and salinities of 1.4 to 57.2 wt.% $NaCl_{eq}$. Inclusions with maximum and minimum salinities and/or homogenization

temperatures were used to plot isochores for each inclusion wafer (e.g. Fig. 2) using the ideal geometric mixing model for the NaCl + H_2O system (Brown and Lamb, 1989). The initial rehydrogenation experiments (A-C) were conducted at 600°C and pressures of 160-180 MPa so that the internal inclusion pressure and confining pressure would be approximately equal during the experiments, so as to minimize the possibility of inclusion decrepitation and/or leakage during the experiments. Additional experiments (D-I) were conducted at 190 MPa and 550°C in an attempt to limit thermal damage of the samples during rehydrogenation (see Appendix Table A.1).

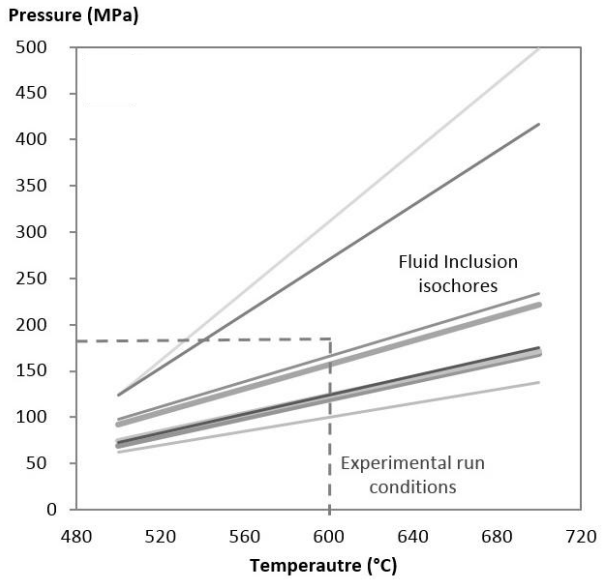

Fig. 2: Representative isochores plotted for fluid inclusions in piece A of sample 07-2406-07A based on measured phase transitions in the system H_2O-NaCl and calculated using the equation-of-state of Brown and Lamb (1989). For these inclusions experimental P-T conditions were selected to lie just above the main grouping of isochores at a run temperature of 600°C and pressure of 180 MPa.

The experimental technique and pressure-capsule design of Mavrogenes and Bodnar (1994) were essentially reproduced in this study. Each quartz wafer sample was sandwiched between two 1 mm thick wafers of pure quartz, which were used to help maintain the integrity of the inclusion wafer on collapse of the Pt capsule. These were placed in a 3 mm ID and ~20 mm long Pt capsule containing water (Fig. 3). This was sealed with an arc welder and loaded into a 5 mm ID diameter, 25-30 mm long Au capsule containing water and chromium nitride (CrN) which was then also welded shut. All experiments were conducted in standard cold-seal pressure vessels (Tuttle, 1949), with water as the pressure medium. Pressure was measured by a Bourdon-tube gauge (uncertainty = ±4.0 Mpa) and temperature was measured by a chromel-alumel thermocouple calibrated against the melting points of Zn and NaCl (uncertainty = ±4.0°C).

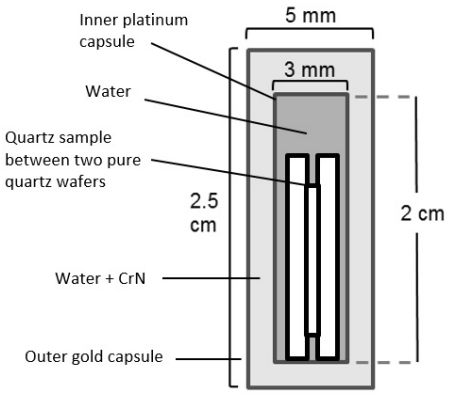

Fig. 3: Double capsule design used for rehydrogenation based on the design of Mavrogenes and Bodnar (1994).

On heating, CrN reacts with water to form chromium oxides, NH_3, N_2, and H_2. Because Pt acts as a semi-permeable membrane with regards to H_2 and Au is very impermeable, the reaction leads to an increase in fH_2 in the outer chamber, leading to diffusion of H_2 into the inner capsule and then into the quartz samples (Chou, 1987). Run times of 167 to 216 hours (Appendix Table A.1) were chosen to maximise the period in which H_2 could diffuse into the inclusions before the CrN had fully reacted with the water. These run times allowed for >90% re-equilibration of H_2 in fluid inclusions located within 20 µm of the sample surface at temperatures of ~600°C (Kats *et al*., 1962).

At the end of each experiment, the sample was cooled and removed from the pressure vessel. Each double-capsule was dried and weighed to verify that there had been no leakage. The Au capsule was then opened carefully in order to remove the inner platinum capsule. A weak smell of ammonia was evident following the first experiment at 216 hours, but was strong following the other runs, indicating that the reaction between CrN and H_2O had not gone to completion and therefore that high fH_2 would have been maintained for the duration of the experiment. The Pt capsules were then opened carefully in order to remove each quartz sample with minimum damage. Samples were examined under plane-polarized light to relocate the previously measured chalcopyrite-bearing fluid inclusions. These were then reanalyzed by microthermometry to check that inclusion integrity had been maintained and to investigate any changes in the solubility of chalcopyrite daughter crystals.

4. Results

4.1 Experimental Complications

The procedure used to measure and rehydrogenate inclusions was subject to a number of problems that made it difficult to relocate the same inclusions before and after the experiments. This may explain why pre- and post-run analysis of the same inclusions was not presented by Mavrogenes and Bodnar (1994).

The first problem was that the anhedral mosaic-textured quartz samples used in this study were susceptible to breaking due to dissolution at grain boundaries and sample crushing during the rehydrogenation experiments (Fig. 4). This led in some cases to complete sample disintegration. However, the majority of samples only broke into ~300-1000 µm pieces, within which the measured chalcopyrite-bearing fluid inclusions could be relocated. It was found that a wafer thickness of ~600 µm was optimal to minimize breakage and to ensure optical clarity of the samples for inclusion observations. The second problem was one of inclusion dimension: most of those that allowed confident identification of triangular chalcopyrite crystals were 10-20 µm in size, but these were prone to decrepitation during pre- or post-rehydrogenation heating experiments. Consequently, only the smaller inclusions that clearly contained chalcopyrite daughters could be used and only a small proportion of these could be successfully relocated after the rehydrogenation experiments (Table 1).

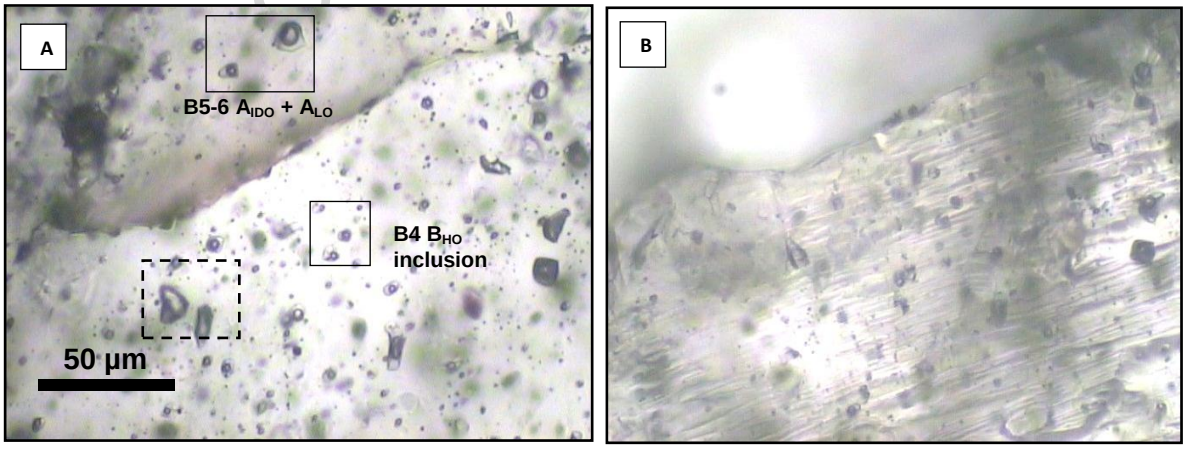

Fig. 4: (A) Before- and (B) after-run photomicrographs of region of interest 3, sample 07-2406-07B, which was affected by the α-β quartz transition during microthermometry to 590°C and was subject to disintegration and fracture annealing during the rehydrogenation experiments. Solid black boxes in A surround inclusions B4-B6, which could not be accurately measured following rehydrogenation.

The third problem was significant restructuring of quartz wafers due to heating of samples through the α-β transition of quartz during microthermometry (Fig. 5) and subsequent heating and cooling of the samples during the rehydrogenation experiments. In accordance with previous studies (Bodnar *et al*., 1989; Hall and Bodnar, 1989), heating through the α-β transition led to mass decrepitation of fluid inclusions and encouraged intergranular fracturing of the samples. The rehydrogenation experiments led to further sample disintegration and resulted in the partial annealing of cracks and further modifications to the shapes of inclusions (e.g. Fig. 4B). This made it extremely difficult to relocate inclusions and in a number of cases the lattice deformation of quartz was so severe that the inclusions could not be re-measured due to decreased transparency of the samples and the formation of apparent sub-parallel deformation features and cracks (e.g. sample 07-2406-07B: Fig. 4B). Because of these difficulties, only a third of the initially measured inclusions were relocated and only 7 out of 87 were re-measured with confidence (Table 1). Unfortunately, no brine inclusions were successfully re-measured.

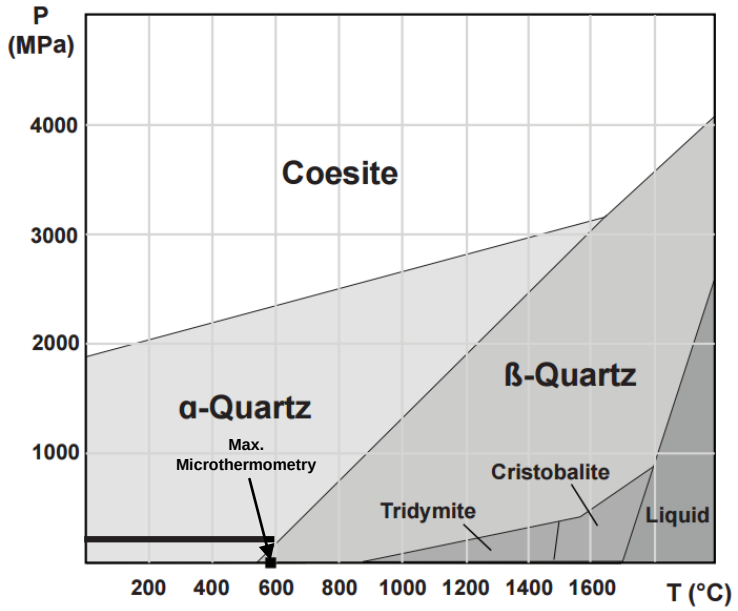

Fig. 5: Simplified phase diagram for SiO_2 polymorphs and liquid. The α-β quartz transition was crossed during microthermometry as samples were heated over 573°C at atmospheric pressure. Experimental conditions (black bar) were near the transition but fell just within the α-quartz stability field.

Table 1: Microthermometric properties of fluid inclusions that were measured before and after rehydrogenation runs.

Before rehydrogenation experiments

Sample Number	Wafer	FLINC	FLINC type	Depth (µm)	Length (µm)	Width (µm)	Bubble Width (µm)	V*f* %	T_mIce (°C)	T_h(L+V→L or V) (°C)	Hom Mode	Salinity (wt.% $NaCl_{eq}$)	Chalcopyrite Dissolution (°C)
07-2406-07	B	**B1**	A_{LO}	25	12.2	7	2.2	25	-8.7	476.4	L	12.5	No
07-2406-07	B	**B3**	A_{LO}	19	10.8	8.2	4.5	35	-12.9	503.1	L	16.8	No
07-2406-07	D	**D3**	A_{IDO}	25	9.3	6.7	4.4	40	-6.3	461.3	L	9.6	No
07-2406-07	F	**F1**	A_{IDO}	16	12.7	9.9	6.0	50	-14.6	518.2	L	18.3	No
07-2406-07	F	**F8**	A_{VO}	19	10.2	8.9	8.9	70	-1.1	444.6	V	1.9	No
07-2406-07	G	**G1**	A_{LO}	4	11.1	9.7	2.2	30	-3.4	403.0	L	5.6	No
07-2406-07	G	**G2**	A_{LO}	7	9.8	9.2	2.2	35	-3.5	408.9	L	5.7	No

After rehydrogenation experiments

Sample Number	Wafer	FLINC	FLINC type	Depth	Length (µm)	Width (µm)	Bubble Width (µm)	V*f* %	T_mIce (°C)	T_h(L+V→L or V) (°C)	Hom Mode	Salinity (wt.% $NaCl_{eq}$)	Chalcopyrite dissolution (°C)
07-2406-07	B	**B1**	A_{LO}	25	12.2	7.4	2.2	25	-8.6	476.3	L	12.4	Partial to 580
07-2406-07	B	**B3**	A_{LO}	19	10.8	8.2	4.5	35	-11.9	502.3	L	15.9	560
07-2406-07	D	**D3**	A_{IDO}	25	9.3	6.7	4.4	40	-6.3	459.1	L	9.6	Partial to 580
07-2406-07	F	**F1**	A_{IDO}	16	12.7	9.9	6.0	50	-14.0	517.9	L	17.8	530
07-2406-07	F	**F8**	A_{VO}	19	10.2	8.9	8.9	70	-1.1	437.2	V	1.9	No change
07-2406-07	G	**G1**	A_{LO}	4	11.1	9.7	2.2	30	-3.4	403.0	L	5.6	Decrepitated
07-2406-07	G	**G2**	A_{LO}	7	9.8	9.2	2.2	35	-3.4	405.8	L	5.6	Decrepitated

Notes: Type 6a vein = quartz-anhydrite-molybdenite-bornite-pyrite vein with no alteration halo present (refer to Fig. 1). Salinities were calculated using the final ice melting temperature (T_mIce) based on the NaCl-H_2O system (Bodnar, 1993; Bodnar and Vityk, 1994). Abbreviations: FLINC = Fluid inclusion. V*f* = Vapor fraction. T_h(L+V→L or V) = Liquid-vapor homogenization temperature (to liquid or vapor phase). Hom mode = Homogenization mode, where L = homogenization to liquid and V = homogenization to vapor. Small changes in salinity and T_h(L+V→L or V) are discussed in the following section. Measured depths are accurate to ±1 µm, T_mIce and and T_h measurements recorded before rehydrogenation are accurate to ±0.1°C and ±0.4°C respectively. The measurements made after rehydrogenation are prone to larger degrees of uncertainty due to difficulty in observing phase changes.

4.2 Fluid Inclusion Microthermometry

Re-examined fluid inclusions were found to contain chalcopyrite daughter crystals that were commonly located in different parts of the inclusion after rehydrogenation, suggesting that they were fully dissolved during the experiments and were re-precipitated during the quench. In general, microthermometry yielded similar results to the pre-experiment data (Table 1). However, the two most saline inclusions appeared to have decreased in salinity (beyond analytical uncertainty) by up to 0.9 wt.% $NaCl_{eq}$ and variations in liquid-vapor homogenization temperatures of up to 7.4°C were also recorded. Changes in the internal pressure of the inclusions at ambient temperature could theoretically affect ice melting phase equilibria. However, each inclusion contains a vapor bubble that almost certainly represents a vapor phase in equilibrium with an aqueous phase and therefore inclusion pressures are likely to be very low (~0.0001 MPa) at the ice melting temperature (e.g. Bodnar *et al*., 1985). This considered, minor variations in salinity and homogenization temperature may be explained by fluid inclusion leakage or minor morphological changes in inclusion shape, which can occur in rehydrogenation experiments conducted over several days (Doppler *et al*., 2013). Alternatively, the largest discrepancies could purely be the result of larger analytical uncertainties as a result of difficulty in observing phase transitions in the damaged samples (e.g. Fig. 4).

4.3 Chalcopyrite Dissolution

Of the seven relocated inclusions, four displayed clear reductions in the size of their chalcopyrite daughter crystals when heated above 460°C (Fig. 7), but full dissolution only occurred in the two most saline inclusions (B3 and F1). Of these, inclusion F1 had the largest volume (Table 2) and therefore provided the best photographic evidence (Fig. 6A). In this inclusion, the chalcopyrite daughter crystal appeared to be fully dissolved by 530°C although the slow dissolution of chalcopyrite made exact measurement of the temperature difficult. After cooling back to room temperature, the chalcopyrite daughter crystals gradually re-precipitated and eventually appeared to be of a similar size to before heating (e.g. Fig. 6A).

In two other inclusions (B1 and D3: Fig. 6B) the chalcopyrite daughter crystals failed to fully dissolve when heated to temperatures of 567 and 580°C, which are close to the heating stage limit. In both inclusions, a decrease in the size of the chalcopyrite daughter crystal was evident above ~460°C (Fig. 6B). By contrast, the chalcopyrite daughter crystal in

the low salinity A_{VO} inclusion did not undergo any noticeable change in size when held at 590°C for an hour (Fig. 6C). Both fluid inclusions in wafer G decrepitated during repeat heating tests, probably because of their lower homogenization temperatures (higher bulk densities) and therefore greater internal overpressures when heated above $Th_{L\text{-}V}$.

Even though only a few fluid inclusions were successfully studied following the rehydrogenation experiments, the samples contained a number of other shallow chalcopyrite-bearing inclusions that showed consistent behavior (Table 2). Chalcopyrite daughter crystals failed to dissolve fully in the fluid inclusions with salinities lower than ~7.5 wt.% $NaCl_{eq}$ (e.g. Fig. 6D) and depths of >20 µm (e.g. Fig. 6G). Due to the fact that heating inclusions through the alpha-beta quartz transition lead to mass decrepitation and surface restructuring (Bodnar *et al*., 1989), brine inclusions were extremely rare in wafers A-C (heated to 600°C). By contrast, a number of brine inclusions were observed in wafers H-I, which were rehydrogenated at 550°C and 190 MPa (Table 2). In accordance with Mavrogenes and Bodnar (1994), the chalcopyrite daughter crystals in three shallow brine inclusions (Fig. 6E-F) readily dissolved as temperatures were raised and held at >500°C. A number of brine inclusions were observed at greater depths from the surface, however, the chalcopyrite crystals in these inclusions failed to dissolve when heated to 550°C (Fig. 6G). This suggests that the concentrations of H_2 were only sufficient for chalcopyrite dissolution near the sample surface (Kats *et al*., 1962).

Due to the extremely small size (<1 µm) of most chalcopyrite daughter crystals and variations in crystal shapes (e.g. Fig. 6) it was difficult to assess the percentage dissolution of chalcopyrite in each fluid inclusion in order to estimate solubility. Furthermore, the extent to which chalcopyrite dissolves is also a function of inclusion composition and degree of rehydrogenation which varies with inclusion depth. Consequently, no attempt was made to define an approximate chalcopyrite solubility curve.

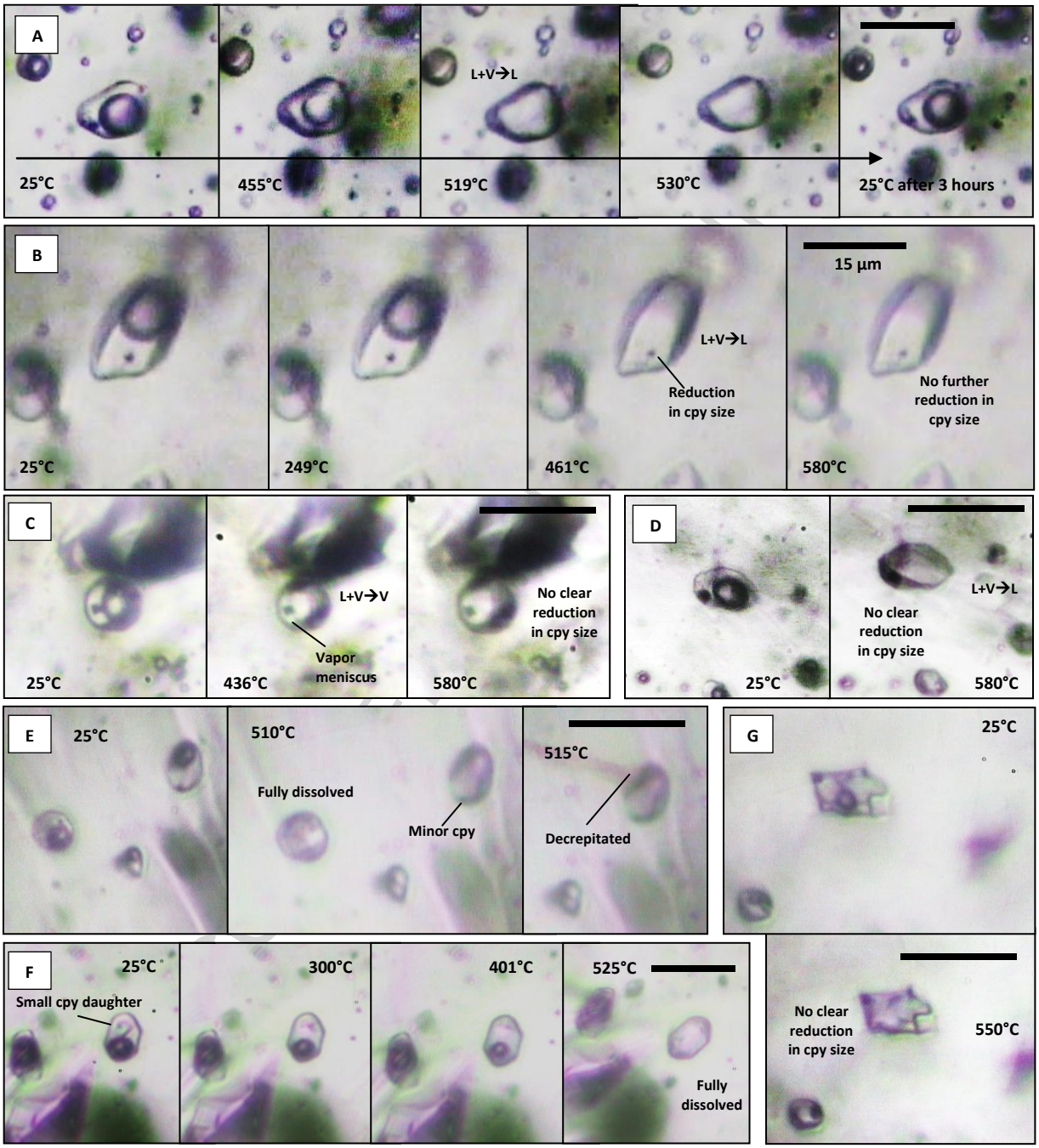

Fig. 6: Photomicrographs showing behavior of chalcopyrite daughter crystals in inclusions with various salinities and depths following rehydrogenation experiments (A) Apparent redissolution of a chalcopyrite daughter crystal at ~530°C (inclusion F1, sample 07-2406-07; see Table 1).The exact temperature of chalcopyrite dissolution was difficult to observe due to a small indentation in the fluid inclusion. (B) Minor reduction in size of daughter crystal as the temperature was increased above 450°C (inclusion D3, sample 07-2406-07). (C) Failed dissolution in a 1.9 wt.% $NaCl_{eq}$ A_V inclusion at a depth of 19 µm (inclusion F8, sample 07-2406-07). (D) Failed dissolution in a 6.8 wt.% $NaCl_{eq}$ A_{IDO} inclusion at a depth of 52 µm (inclusion FA1 – not measured before rehydrogenation). (E-F) Successful redissolution of chalcopyrite daughter crystals in dense brine inclusions (E = inclusions HA5 and HA6, F = inclusions IA1 - not measured before rehydrogenation). (G) Failed redissolution of chalcopyrite in a deeper (47 µm) brine inclusion (inclusion IA2– not measured before rehydrogenation, see Table 2). Scale bars = 15 µm.

Table 2: Microthermometric properties of fluid inclusions that were only measured after rehydrogenation.

Sample Number	FLINC	FLINC type	Depth	V*f* (%)	T_h(total) (°C)	Hom Mode	Salinity (wt.% $NaCl_{eq}$)	Chalcopyrite Dissolution (°C)
07-2406-07	**BA1**	A_{LO}	12	25	429.9	L	9.0	550.7
07-2406-07	**BA2**	A_{LO}	19	30	423.3	L	8.1	540.9
07-2406-07	**BA3**	A_{VO}	7	70	400.2	V	1.3	No Change
07-2406-07	**FA1**	A_{IDO}	14	45	455.4	L	6.8	No Change
07-2406-07	**FA2**	A_{VO}	20	70	399.0	V	0.9	No Change
07-2406-07	**FA3**	A_{LO}	11	30	408.8	L	4.2	No Change
07-2406-07	**FA4**	A_{IDO}	10	45	420.3	L	8.0	Partial >550
07-2406-07	**HA1**	A_{LO}	9	35	408.3	L	7.9	530.2
07-2406-07	**HA2**	A_{LO}	14	35	400.8	L	5.4	Partial 590
07-2406-07	**HA3**	A_{VO}	16	80	396.1	V	1.0	No Change
07-2406-07	**HA4**	A_{IDO}	13	60	430.4	L	5.5	Partial 590
07-2406-07	**HA5**	B_{HO}	20	20	386.2	L	33.0	510.5
07-2406-07	**HA6**	B_{HO}	24	20	388.5	L	33.2	Partial >515
07-2406-07	**IA1**	B_{HO}	12	25	450.5	L	37.2	525.1
07-2406-07	**IA2**	B_{HO}	47	20	390.5	L	>54.0	No Change
07-2406-07	**HA3**	A_{IDO}	13	50	432.4	L	8.7	560.3
07-2406-07	**HA4**	A_{IDO}	21	50	432.4	L	6.4	Partial >580

Notes: Wafer B was equilibrated at 600°C and 160 MPa, whereas the other wafers were equilibrated at 550°C and 190 MPa. Salinities were calculated using the final ice melting temperature (T_m Ice) based on the NaCl-H_2O system (Bodnar, 1993; Bodnar and Vityk, 1994). Abbreviations: FLINC = Fluid inclusion. V*f* = Vapor fraction. T_h(L+V→L or V) = Liquid-vapor homogenization temperature (to liquid or vapor phase). Hom mode = Homogenization mode, where L = homogenization to liquid and V = homogenization to vapor. Measured depths are accurate to ±1 µm, all salinity measurements had an uncertainty of >0.5 wt.% $NaCl_{eq}$ and T_h measurements had an uncertainty of ±0.4°C.

5. Discussion

The rehydrogenation experiments confirm that increasing fH_2 in fluid inclusions via diffusion through quartz leads to the partial or total dissolution of chalcopyrite daughter minerals that were previously insoluble. However, the results from this and the previous study (Mavrogenes and Bodnar, 1994) have only documented this effect for moderate to high salinity inclusions (>~7.5 wt.% $NaCl_{eq}$). Here, we find that chalcopyrite crystals in rehydrogenated, low salinity A_{IDO} and low density A_{VO} inclusions show negligible changes in size when heated to temperatures considerably higher than their interpreted liquid-vapor homogenization temperatures (Fig. 6, Table 2). This suggests that factors other than H_2 loss are important controls on chalcopyrite solubility in these inclusion types.

Mavrogenes and Bodnar (1994) did not address the reactions responsible for the (renewed) dissolution of chalcopyrite, perhaps due to the absence of a technique that could ascertain accurately the compositions of the inclusions. In contrast, fluid inclusions in the vein types used in this study have been studied previously using PIXE (Cannell, 2004) and LA-ICP-MS analysis (Klemm *et al*., 2007; Vry, 2010). These studies showed that all fluid inclusion types are dominated by Na, Cl, K, Ca, Fe, Mn, Cu, Pb and As, all of which correlate positively with inclusion salinity.

The highest Cu concentrations at El Teniente were recorded for high salinity brine inclusions. This is likely to be due to the preferential complexation of Cu as highly soluble $CuCl^0$ and $[CuCl_2]^-$ species as proposed in a number of solubility (Candela and Holland, 1984, 1986; Bai and Koster van Groos, 1999; Archibald *et al*. 2002; Simon *et al*., 2006) and speciation studies (Mavrogenes *et al*., 2002; Berry *et al*, 2006, 2009). Despite this, Cu concentrations were also commonly elevated in several low salinity (<2.0 wt.% $NaCl_{eq}$), liquid or vapor inclusions at El Teniente (Vry, 2010). This suggests that significant amounts of Cu may also be dissolved as $[Cu(H_2O)_6]^{2+}$ in vapors with high fH_2O (Mavrogenes *et al*., 2002), or as HS^- complexes including $[Cu(HS)_2]^-$ in relatively reduced, sulfur-rich fluids (Heinrich *et al*. 1999; Mountain and Seward, 2003; Simon *et al*., 2006; Pokrovski *et al*., 2008; Seo *et al*., 2009; Landtwing *et al*., 2010). As a result, the solubility of chalcopyrite daughter crystals in quartz-hosted inclusions may be controlled by several different equilibria, some of which may be influenced by fH_2 and some of which may not.

The oxidation states of Cu and Fe in chalcopyrite are predominantly +1 and +3 respectively (e.g. van der Laan *et al*., 1992; Rickard and Cowper, 1994; Pearce *et al*., 2006) and the predominant oxidation state of Fe in solution at elevated temperatures and a range of salinities is likely to be +2 (e.g. Seyfried and Ding, 1993; Liu *et al*., 2002). Given this, and assuming the proposed complexes of Cu in solution noted above, the likely equilibria that govern the solubility of chalcopyrite in fluid inclusions are:

$$2Fe^{2+} + 2Cu^{+} + 4HS^{-} = 2CuFeS_2 + H_2 + 2H^{+} \text{ .....or} \quad (1)$$

$$2Fe^{2+} + 2Cu^{+} + 4H_2S = 2CuFeS_2 + H_2 + 6H^{+} \quad (2)$$

According to these reactions, if H_2 is produced by the crystallization of chalcopyrite and subsequently lost from fluid inclusions post-entrapment, then the back reaction and dissolution of chalcopyrite will be prevented when the inclusion is heated back to the trapping conditions. Obviously, the temperature-dependence of sulfide solubility (implicit in the precipitation of sulfide daughter crystals within inclusions) means that heating would always be required to redissolve a chalcopyrite crystal. Rehydrogenation and then heating of such inclusions, clearly, would allow chalcopyrite redissolution to take place according to either of these reactions.

The successful dissolution of chalcopyrite daughter crystals in the most saline inclusions (Fig. 6; Tables 1-2) suggests that the experimental technique was successful in permitting the reversal of reaction 1 or 2 on heating. The incomplete dissolution of chalcopyrite in the two relocated moderate salinity inclusions is attributed to the fact that they were at greater depths (25 µm; Table 2) such that insufficient H_2 was able to diffuse back into them during rehydrogenation. Based on previous experimental estimates (Kats *et al*., 1962; Mavrogenes and Bodnar, 1994) inclusions at these depths would require run times of at least 330 hours to achieve 95% H_2 reequilibration.

The failure of the chalcopyrite daughter crystals to dissolve in the rehydrogenated vapor inclusions, despite their equivalent depths to the more saline liquid inclusions, requires explanation. If porphyry vapors are trapped at high temperature (>400°C), they will produce significant H^{+} via the dissociation of acids and the disproportionation of magmatic sulfur dioxide (e.g. Giggenbach, 1992; Rye, 1993; Heinrich *et al*., 2004), which both occur in

response to decreases in temperature and pressure (Meyer and Hemley, 1967; Reed and Rusk, 2001; Reed *et al*., 2005; Rusk *et al*., 2008):

$$H_2SO_4 = H^+ + HSO_4^- = 2H^+ + SO_4^{2-} \quad (3)$$

$$HCl = H^+ + Cl^- \quad (4)$$

$$4SO_2 + 4H_2O = H_2S + 3HSO_4^- + 3H^+ \quad (5)$$

In the presence of a gradient in chemical potential (e.g. pH difference), H^+ can freely diffuse out of fluid inclusions as long as charge balance is maintained by the inward diffusion of univalent metal ions with ionic radii small enough to pass through the 1 Å diffusion channels in quartz (Mortley, 1969; White, 1970: Fig. 7). Recent experiments have demonstrated that several cations, including Li^+, Na^+, Cu^+ and Ag^+ have the potential to rapidly diffuse through quartz (Li *et al*., 2009; Zajacz *et al*., 2009; Lerchbaumer and Audétat, 2012; Seo and Heinrich, 2013) providing a mechanism for balancing H^+. In particular, reequilibration experiments have indicated that Cu concentrations could be significantly modified in porphyry fluid inclusions by such a mechanism (Lerchbaumer and Audétat, 2012). Inward diffusing Cu^+ combines with dissolved S (as HS^- or H_2S) and Fe^{2+} to form chalcopyrite. In accordance with reactions 1-2, this generates more H^+ perpetuating further exchange of H^+ for incoming Cu^+ (Seo and Heinrich, 2013).

Inward Cu^+ diffusion can continue as long as there is reduced sulfur in the inclusion to precipitate chalcopyrite. This explains why S-rich vapor inclusions commonly have Cu/S molar ratios that reflect the ~1:1 mass ratio of Cu and S in chalcopyrite (Seo *et al*., 2009). The strong partitioning of acid volatiles and sulfur species into the vapor phase (e.g. Burnham and Ohmoto, 1985; Heinrich *et al*., 1999) suggest that the opaque daughter crystals in these inclusions are likely to be the result of post-entrapment inward diffusion of Cu^+ (Fig. 8C). By contrast, the non-dissolvable chalcopyrite daughter crystals in the partitioned brine inclusions, which dissolve after rehydrogenation, are explained by the favorable partitioning of Cu into the dense hypersaline fluids and subsequent H_2 loss (Fig. 7).

At El Teniente the vapor and brine inclusions are interpreted to have been produced by the phase separation of intermediate density fluids with salinities of ~7.0 wt.% $NaCl_{eq}$ that boiled as temperatures dropped to ~390°C (Spencer *et al*., 2013). Preliminary LA-ICP-MS and microthermometric analyses reveal that the parental fluids had typical Cu concentration

of ~3000 ppm and produced brines with typical salinities of ~43.3 wt.% $NaCl_{eq}$ and Cu concentrations of ~10000 ppm (Fig. 7A). In accordance with Dreisner (2007) a phase separated vapor in equilibrium with a brine at this temperature should have a salinity of ~ 0.01 wt.% $NaCl_{eq}$. This equates to an inferred vapor/brine mass ratio of ~5.7 when considering an input fluid of ~7.0 wt.% $NaCl_{eq}$ (Fig. 7B). The average Cu concentration of 1760 ppm in the phase separated vapors suggests that $DCu^{vapor/brine}$ values of ~0.176 are typical for the main mineralization fluids at El Teniente. This only slightly exceeds recent $DCu^{vapor/brine}$ values of 0.11 to 0.15 calculated by Lerchbaumer and Audétat (2012) for unmodified porphyry ore fluids using similar vapor/brine mass ratios of 4–9.

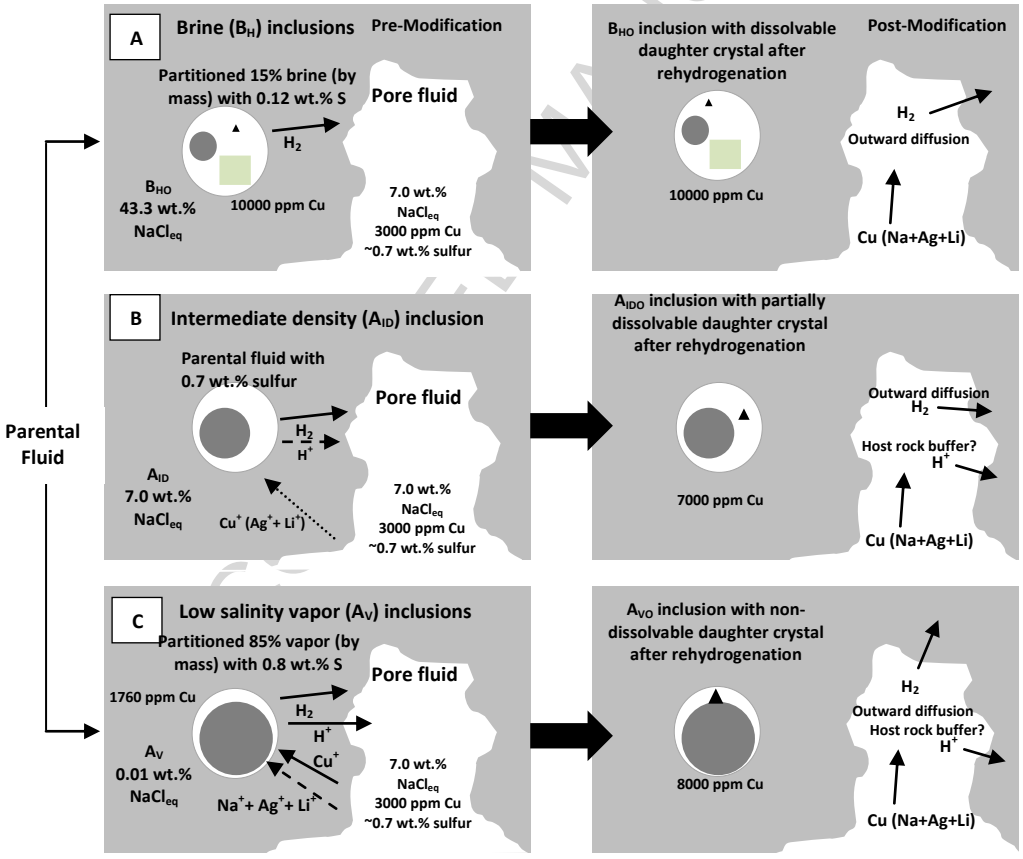

Fig. 7. Schematic sketch showing the post-entrapment modification of H_2, Cu^+ and H^+ concentrations in (A) high salinity brine inclusions, (B) moderate salinity, intermediate density inclusions and (C) low density, S-rich vapor inclusions hosted in quartz in equilibrium with an ore fluid. The intermediate density inclusions are interpreted to represent parental fluids for the partitioned vapor and brine assemblages (Spencer *et al.*, 2013). Outward H^+ diffusion relies on a gradient in fluid acidity and permits inward Cu^+ diffusion to maintain a charge balance. Incoming Cu is precipitated as chalcopyrite leading to net Cu gain. Due to the high initial H_2S concentrations of vapor inclusions they can acquire large quantities of Cu. Figure after Lerchbaumer and Audétat (2012). Fluid inclusion and external fluid salinities and compositions are based on previous fluid inclusion studies (Cannell, 2004; Klemm *et al.*, 2007; Vry, 2010) and unpublished LA-ICP-MS data for El Teniente.

Boiling assemblages are particularly abundant in quartz-chalcopyrite type 6b veins (Fig. 8a) and quartz-anhydrite-chalcopyrite type 8 veins (Fig. 8b) with sericitic halos. These veins were formed by the same fluids as they migrated outward and upward and cooled (Spencer *et al*., 2015). In the type 6b veins the vapor inclusions contain Cu concentrations of up to 8000 ppm (Fig. 8a), suggesting that they may be the product of post-entrapment Cu diffusion into vapors that contained approximately 0.8 wt.% S (Fig. 7C). These concentrations are similar to the S concentrations of up to 1 wt.% recorded in vapor inclusions associated with Cu mineralization of the Mole granite, Australia (Heinrich *et al*., 1999). By contrast, vapor inclusions in the type 8 veins record a far lower average Cu concentration of ~200 ppm and the apparent boiling assemblages yield a lower $DCu^{vapor/brine}$ value of ~0.11, similar to those reported by Lerchbaumer and Audétat (2012). This suggests that the vapor inclusions in these veins may have been less prone to post-entrapment Cu enrichment. The presence of intense sericitic alteration in the outboard type 8 veins indicates that they formed in the presence of acidic fluids produced by acid dissociation as temperatures dropped below 400°C. This, and the presence of abundant chalcopyrite in the type 8 veins implies that most vapor inclusions were trapped in the presence of relatively Cu-poor and H^+-rich ore fluids. Consequently, the average $DCu^{vapor/brine}$ value of ~0.11 found for boiling assemblages in the type 8 veins may reflect the true partitioning behavior of Cu at El Teniente.

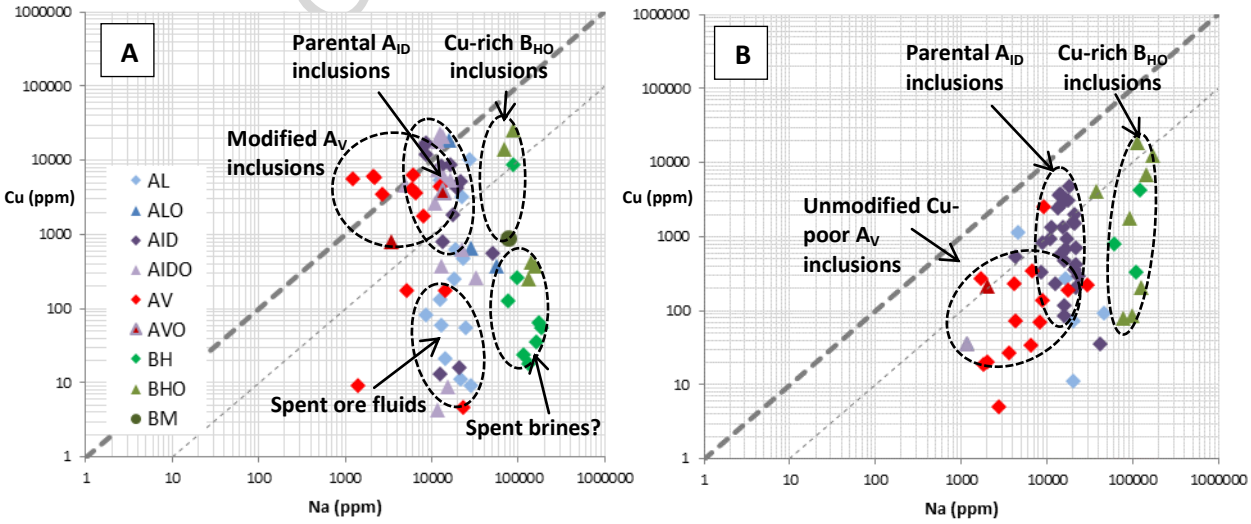

Fig. 8. Individual fluid inclusion LA-ICP-MS data for different fluid inclusion types in (A) quartz-chalcopyrite type 6b veins and (B) sericite altered quartz-chalcopyrite type 8 veins at El Teniente. Refer to Fig. 1 for inclusion nomenclature. Data were collected for veins from several mineralized intrusions. Dashed diagonal lines = Cu/Na concentration ratios of 1 and 0.1.

6. Conclusions

This study finds that the experimental technique of Mavrogenes and Bodnar (1994) can be used to diffuse H_2 back into fluid inclusions without modifying inclusion microthermometric properties. Rehydrogenation experiments increased chalcopyrite daughter crystal solubility in moderate salinity inclusions, highlighting the importance of H_2 loss for preventing chalcopyrite daughter crystal dissolution. The technique was only successful for shallow inclusions due to the relationship between the depth of H_2 diffusion through quartz and time. The failed redissolution of chalcopyrite in rehydrogenated, low salinity vapor inclusions is interpreted to be the result of post-entrapment Cu gain due to their high initial reduced S contents and the presence of acid-generating species, which led to the precipitation of "excess" chalcopyrite.

In accordance with Lerchbaumer and Audétat (2012), the consequence of this is that Cu concentrations measured by LA-ICP-MS in quartz-hosted, S-rich vapor inclusions are often likely to be modified by post-entrapment, at least in porphyry deposits where high Cu pore fluids may be present throughout much of the life of the system. Preliminary LA-ICP-MS data suggest that Cu concentrations in vapor inclusions at El Teniente from the main quartz-sulfide vein stage are likely to have been enhanced by around one order of magnitude by this process. Results from the sericite-stable vein stage suggest that diffusional Cu gain may be less pronounced in the later (phyllic-argillic alteration) stages of the evolution of porphyry systems where the ambient fluids are more acidic, thereby hindering outward H^+ diffusion. This also suggests that Cu diffusion principally occurs on the timescale of an active hydrothermal system (tens to hundreds of thousands of years) rather than requiring geological timescales. In fact, experimental data show that Cu diffusion into inclusions can occur over a matter of days so that, in natural systems, predisposed inclusions may effectively be modified as soon as they are trapped. Future analyses of rehydrogenated inclusions using Raman spectroscopy may provide insight into the H_2 content of the vapor bubbles and H_2 variability between inclusion types, while PIXE analyses may determine the distribution of Cu in different phases within each inclusion type.

The selective, post-entrapment modification of Cu concentrations in vapor inclusions undermines the importance of phase separated vapors as a key agent of Cu transport and deposition in porphyry and overlying epithermal systems (e.g. Roedder, 1971; Heinrich *et al*.,

1999; Klemm *et al*., 2007; Rusk *et al*., 2004; Landtwing *et al*., 2010). Based on our observations we suggest that parental intermediate density fluids play the most important role in transporting Cu into the shallow crust, whereas phase-separated vapors and brines, which are subordinate in terms of total mass, may play relatively similar roles in transporting and depositing Cu in the porphyry environment. The upward transition of some porphyry systems into vapor-dominated epithermal systems (e.g. Hedenquist and Lowenstern, 1994; Sillitoe, 2010; Lecumberri-Sanchez *et al*., 2013) implies a potential increase in the importance of vapors for transporting Cu in these shallower hydrothermal environments.

Acknowledgements

We are extremely grateful to the members of CODELCO Superintendencia de Geología, El Teniente, especially Patricio Zuñiga, Jose Seguel and Felipe Celhay for providing access to the mine, drillcore samples, grade data and valuable insights into the geological evolution of El Teniente. We would like to thank the Department of Earth Science and Engineering, Imperial College London for granting a Ph.D. scholarship to the primary author, and the Institute of Materials, Minerals and Mining (IOM3 bursary) and the Society of Economic Geologists (Hugh E. McKinstry Fund) for additional financial support. Finally, we would like to thank Jeremy Fein, Bob Bodnar and an anonymous reviewer for their detailed reviews of this work.

Appendix

Table A.1: Summary of rehydrogenation experimental conditions.

Sample Number	Run Number	Wafer Code	T (°C)	P (MPa)	Duration (h)
07-2406-07	L-fO_2-1	A	600	180	216
07-2406-07	L-fO_2-2	B	600	160	168
07-2406-07	L-fO_2-3	C	600	160	167
07-2406-07	L-fO_2-4	D	550	190	192
07-2406-07	L-fO_2-5	E	550	190	192
07-2406-07	L-fO_2-6	F	550	190	192
07-2406-07	L-fO_2-7	G	550	190	192
07-2406-07	L-fO_2-15	Failed	550	190	191
07-2406-07	L-fO_2-16	H	550	190	191
07-2406-07	L-fO_2-17	I	550	190	191

Notes: Wafer codes were given to successful runs in which fluid inclusions could be measured following rehydrogenation. L-fO_2-15 disintegrated during the run.

References

Anderko A., and Pitzer, K.S., 1993, Equation-of-state representation of phase equilibria and volumetric properties of the system NaCl-H_2O above 573 K: Geochimica et Cosmochimica Acta, v. 57, p. 1657-1680.

Archibald, S.M., Migdisov, A.A., and Williams-Jones, A.E., 2002, An experimental study of the stability of copper chloride complexes in water vapor at elevated temperatures and pressures: Geochimica et Cosmochimica Acta, v. 66, p. 1611-1619.

Bai, T.B., and Koster van Groos, A.F.K., 1999, The distribution of Na, K, Rb, Sr, Al, Ge, Cu, W, Mo, La, and Ce between granitic melts and coexisting aqueous fluids: Geochimica et Cosmochimica Acta, v. 63, p. 1117–1131.

Becker, S.P., Fall, A., and Bodnar, R.J., 2008, Synthetic Fluid Inclusions. XVII. PVTX Properties of high salinity H_2O-NaCl Solutions (>30 wt% NaCl): Application to Fluid Inclusions that Homogenize by Halite Disappearance from Porphyry Copper and Other Hydrothermal Ore Deposits: Economic Geology, v. 103, p. 539-554.

Berry, A.J, Hack, A.C., Mavrogenes, J.A., Newville, M., and Sutton, S.R., 2006, A XANES study of Cu speciation in high-temperature brines using synthetic fluid inclusions: American Mineralogist, v. 91, p. 1773-1782.

Berry, A.J., Harris, A.C., Kamenetsky, V.S., Newville, M., and Sutton, S.R., 2009, The speciation of copper in natural fluid inclusions at temperatures up to 700 ˚C: Chemical Geology, v. 259, p. 2-7.

Bischoff, J.L., and Pitzer, K.S., 1989, Liquid-vapour relations for the system NaCl-H_2O: summary of the PTX surface from 300ºC to 500°C: American Journal of Science, v. 289, p. 217-248.

Bodnar, R. J., 1992. Can we recognise magmatic fluid inclusions in fossil hydrothermal systems based on room temperature phase relations and microthermometric behaviour?. Geological Survey of Japan, v. 279, p. 26-30.

Bodnar, R.J., 1993, Revised equation and table for determining the freezing point depression of H_2O-NaCl solutions: Geochimica et Cosmochimica Acta, v. 57, p. 683-684.

Bodnar, R.J., and Sterner, S.M., 1985, Synthetic Fluid Inclusion in Natural Quartz. II. Applications to PVT studies: Geochimica et Cosmochimica Acta, v. 49, p. 1855-1859.

Bodnar, R.J., and Vityk, M., 1994, Interpretation of microthermometric data for H2O-NaCl fluid inclusions. In: Short Course of Working Group (IMA) in "Inclusions in Minerals": Pontignano-Siena: p. 117-130.

Bodnar, R.J., Burnham, C.W., and Sterner, S.M., 1985, Synthetic fluid inclusions in natural quartz. III. Determination of phase equilibrium properties in the system H_2O-NaCl to 1000ºC and 1500 bars: Geochimica et Cosmochimica Acta, v. 49, p. 1861-1873.

Bodnar, R.J., Binns P.R., and Hall, D.L., 1989, Synthetic fluid inclusions-Vl Quantitative evaluation of the decrepitation behavior of fluid inclusions in quartz at one atmosphere confining pressure: Journal of Metamorphic Geology, v. 7, p. 229-242.

Brown, P.E., and Lamb, W.M., 1989, P -V-T properties o f fluids in the system H_2O-CO_2-NaCl: New graphical presentations and implications for fluid inclusion studies: Geochimica et Cosmochimica Acta, v. 53, p. 1209-1221.

Candela, P.A., and Holland, H.D., 1984, The partitioning of copper and molybdenum between silicate melts and aqueous fluids: Geochimica et Cosmochimica Acta, v. 48, p. 373–380.

Candela, P.A., and Holland, H.D., 1986, A mass transfer model for copper and molybdenum in magmatic-hydrothermal systems; the origin of porphyry-type ore deposits: Economic Geology, v. 81, p. 1-9.

Cannell, J., 2004, El Teniente porphyry copper-molybdenum deposit, central Chile: Unpublished Ph.D. thesis, Hobart, Australia, University of Tasmania, 299 p.

Cannell, J., Cooke, D.R., Walshe, J.L., and Stein, H., 2005, Geology, mineralization, alteration, and structural evolution of the El Teniente porphyry Cu-Mo deposit: Economic Geology, v. 100, p. 979–1003.

Chou, I-M., 1987, Phase relations in the system NaCl-KCI-H_2O. Part III: Solubilities of halite in vapor-saturated liquids above 445°C and redetermination of phase equilibrium properties in the system NaCl-H_20 to 1000°C and 1500 bars: Geochimica et Cosmochimica Acta, v. 51, p. 1965–1975.

Doppler, G., Bakker, R.J., and Baumgartner, M., 2013, Fluid inclusion modification by H2O and D2O diffusion: the influence of inclusion depth, size, and shape in re-equilibration experiments: Contributions to Mineralogy and Petrology, v. 165, p. 1259–1274.

Driesner, T., 2007, The System H_2O-NaCl. II. Correlation formulae for phase relations in temperature-pressure-composition space from 0 to 1000°C, 0 to 5000 bar, and 0 to 1 X_{NaCl}: Geochimica et Cosmochimica Acta, v. 71, p. 4902–4919.

Gibbs, R.E., 2012, Structure of alpha quartz: Proceedings of the Royal Society of London, v. 110, p. 443–455.

Giggenbach, W.F., 1992, Magma degassing and mineral deposition in hydrothermal systems along convergent plate boundaries: Economic Geology, v. 87, p. 1927−1944.

Goh, S.W., Buckley, A.N., and Lamb, R.N., Rosenberg, R.A., and Moran, D., 2006, The oxidation states of copper and iron in mineral sulfides, and the oxides formed on initial exposure of chalcopyrite and bornite to air: Geochimica et Cosmochimica Acta v. 70, p. 2210–2228.

Hack, A.C., and Mavrogenes, J.A., 2006, A synthetic fluid inclusion study of copper solubility in hydrothermal brines from 525 to 725 °C and 0.3 to 1.7 GPa: Geochimica et Cosmochimica Acta, v. 70, p. 3970–3985.

Hall, D. L., 1989, Fluid evolution during metamorphism and uplift of the massive sulfide deposits at Ducktown, Tennessee, USA. Unpublished Ph.D. thesis, Virginia Polytechnic Institute and State University.

Hall, D.L., and Bodnar, R.J., 1989, Comparison of fluid inclusion decrepitation and acoustic emission profiles of Westerley granite and Sioux quartzite: Tectonophysics, v. 168, 283-296.

Hall, D.L., and Bodnar, R.J., 1990, Methane in fluid inclusions from granulites: A product of hydrogen diffusion? Geochimica et Cosmochimica Acta, v. 54, 641–651.

Hall D.L., Bodnar R.J., and Craig, J.R., 1991, Evidence for post entrapment diffusion of hydrogen into peak metamorphic fluid inclusions from the massive sulfide deposits at Ducktown, Tennessee: American Mineralogist, v. 76, p. 1344–1355.

Hedenquist, J.W., and Lowenstern, J.B., 1994, The role of magmas in the formation of hydrothermal ore deposits: Nature, v. 370, p. 519−527.

Heinrich, C.A., Günther, D., Audétat, A., Ulrich, T., and Frischknecht, R., 1999, Metal fractionation between magmatic brine and vapor, determined by micro-analysis of fluid inclusions: Geology, v. 27, p. 755–758.

Heinrich, C.A., Driesner, T., Stefansson, A., and Seward, T.M., 2004, Magmatic vapor contraction and the transport of gold from the porphyry environment to epithermal ore deposits: Geology, v. 32, p. 761−764.

Hemley, J.J., Cygan, G.L., Fein, J.B., Robinson, G.R., and d'Angelo, V.M., 1992, Hydrothermal ore-forming processes in the light of studies in rock buffered systems: I. Iron-copper-zinc-lead sulphide solubility relations: Economic Geology, v. 87, p. 1–22.

Kats, A., Haven, Y., and Stevels, J.M. 1962, Hydroxyl groups in alpha quartz: Physics and Chemistry of Glasses, v. 3, p. 69-75.

Klemm, L.M., Pettke, T., Heinrich, C.A., and Campos, E., 2007, Hydrothermal evolution of the El Teniente deposit, Chile: Porphyry Cu-Mo ore deposition from low-salinity magmatic fluids: Economic Geology, v. 102, p. 1021−1045.

Landtwing, M.R., Furrer, C., Redmond, P.B., Pettke, T., Guillong, M., and Heinrich, C.A., 2010, The Bingham Canyon porphyry Cu–Mo–Au deposit. III. Zoned copper-gold ore deposition by magmatic vapor expansion: Economic Geology, v. 105, p. 91−118.

Lecumberri-Sanchez, P., Newton, M.C., Westman, E.C., Kamilli, R.J., Canby, V.M., and Bodnar, R.J., 2013, Temporal and spatial distribution of alteration, mineralization and fluid inclusions in the transitional high-sulfidation epithermal–porphyry copper system at Red Mountain, Arizona: Journal of Geochemical Exploration, v. 125, p. 80-93.

Lerchbaumer and Audétat, 2012, High Cu concentrations in vapor-type fluid inclusions: an artifact?: Geochimica et Cosmochimica Acta, v. 88, p. 255–274.

Li Y., Audetat, A., Lerchbaumer, L., and Xiong, X.L., 2009, Rapid Na, Cu exchange between synthetic fluid inclusions and external aqueous solutions: evidence from LA-ICP-MS analysis: Geofluids, v. 9, p. 321-329.

Liu, W.H., Brugger, J., McPhail, D.C., and Spiccia, L., 2002, A spectrophotometric study of aqueous copper(I)-chloride complexes in LiCl solutions between 100 and 250 °C: Geochimica et Cosmochimica Acta, v. 66, p. 3615–3633.

Mavrogenes, J.A., and Bodnar, R.J., 1994, Hydrogen movement into and out of fluid inclusions in quartz—experimental evidence and geologic implications: Geochimica et Cosmochimica Acta, v. 58, p.141–148.

Mavrogenes, J.A., Williamson, M.A., and Bodnar, R.J., 1992, Cu, Fe, and S concentrations in magmatic/hydrothermal fluids: Evidence from natural and synthetic fluid inclusions (abs): GSA Abstract Programme, v. 24, p. A- I44.

Mavrogenes, J.A., Berry, A.J., Newville, M., and Sutton, S.R., 2002, Copper speciation in vapor-phase fluid inclusions from the Mole Granite, Australia: American Mineralogist, v. 87, p. 1360–1364.

Meyer, C., and Hemley, J.J., 1967, Wall rock alteration, in: Barnes, H.L., ed., Geochemistry of Hydrothermal Ore Deposits. New York, Holt, Rinehart and Winston, Inc., p. 166–232.

Mountain, B.W., and Seward, T.M., 2003, Hydrosulfide complexes of copper (I): Experimental confirmation of the stoichiometry and stability of $Cu(HS)^{2-}$ to elevated temperatures: Geochimica et Cosmochimica Acta, v. 67, p. 3005-3014.

Morgan, G.B., Chou, I.M., Pasteris, J.D., and Olsen, S.N., 1993, Re-equilibration of CO_2 fluid inclusions at controlled hydrogen fugacities: Journal of Metamorphic Geology, v. 11, p. 155–164.

Mortley, W.S., 1969, Diffusion paths in quartz: Nature, v. 221, p. 359-360.

Pearce, C.I., Pattrick, R.A.D., Vaughan, D.J., Henderson, C.M.B., and van der Laan, G., 2006, Copper oxidation state in chalcopyrite: Mixed Cu d^9 and d^{10}characteristics Geochimica et Cosmochimica Acta, v. 70, p. 4635–4642.

Pokrovski, G.S., Borisova, A.Y., and Harrichoury, J-C., 2008, The effect of sulfur on vapor-liquid fractionation of metals in hydrothermal systems: Earth and Planetary Science Letters, v. 266, p. 345–362.

Reed, M., and Rusk, B., 2001, Insights into supercritical hydrothermal processes from numerical models of potassic hydrothermal alteration, and SEM-CL imaging of vein quartz at Butte, Montana, in Toshiyuki, H., ed., Proceedings from the Workshop on Potential Thermal Extraction from Deep-seated Rock Masses: Sendai, Japan, Tohoku University, p. 37–53.

Reed, M.H., Rusk, B., Palandri, J., and Dilles, J., 2005, The Butte hydrothermal system: One magmatic fluid yielded all vein types [abs]: Geological Society of America Abstracts with Programs, v. 37, p. A315.

Rickard, D., and Cowper, M., 1994, Kinetics and mechanism of chalcopyrite formation from Fe(II) disulphide in aqueous solution (<200°C): Geochimica et Cosmochimica Acta, v. 58, p. 3795–3802.

Roedder, E., 1984, Fluid inclusions: an introduction to studies of all types of fluid inclusions, gas, liquid, or melt, trapped in materials from earth and space: Reviews in Mineralogy, v. 12, Mineralogical Society of America, Washington D.C.: 646 pp.

Rusk, B.G., Reed, M.H., Dilles, J.H., Klemm, L.M., and Heinrich, C.A., 2004, Compositions of magmatic hydrothermal fluids determined by LA-ICP-MS of fluid inclusions from the porphyry copper–molybdenum deposit at Butte, Montana: Chemical Geology, v. 210, p. 173–199.

Rusk, B.G., Reed, M.H., and Dilles, J.H., 2008, Fluid inclusion evidence for magmatic-hydrothermal fluid evolution in the porphyry copper-molybdenum deposit at Butte, Montana: Economic Geology, v. 103, p. 307−334.

Rye, R.O., 1993, The evolution of magmatic fluids in the epithermal environment: the stable isotope perspective: Economic Geology, v. 88, p. 733−753.

Seo, J.H., Guillong, M., and Heinrich, C.A., 2009, The role of sulfur in the formation of magmatic–hydrothermal copper–gold deposits: Earth and Planetary Science Letters, v. 282, p. 323–328.

Seo, J.H., and Heinrich, C.A., 2013, Selective copper diffusion into quartz-hosted vapor inclusions: Evidence from other host minerals, driving forces, and consequences for Cu–Au ore formation: Geochimica et Cosmochimica Acta v. 113, p. 60–69.

Seyfried, W.E., Jr, and Ding, K., 1993, The effect of redox on the relative solubilities of copper and iron in Cl-bearing aqueous fluids at elevated temperatures and pressures: An experimental study with application to subseafloor hydrothermal systems: Geochimica et Cosmochimica Acta, v. 57, p. 1905-1917.

Simon, A.C., Pettke, T., Candela, P.A., Piccoli, P.M., and Heinrich, C.A., 2006, Copper partitioning in a melt–vapor–brine–magnetite–pyrrhotite assemblage: Geochimica et Cosmochimica Acta, v. 70, p. 5583–5600.

Sillitoe, R.H., 2010, Porphyry copper systems: Economic Geology, v. 105, p. 3–41.

Spencer, E.T., Wilkinson, J.J., Seguel, J., and Berry, A.J., 2013, The roles of intermediate density fluids, vapours and brines in the formation of Mo-rich porphyries [abs]: MDSG annual meeting abstract volume, Leicester, UK.

Spencer, E.T., Wilkinson, J.J., Creaser, R.A., and Seguel, J., 2015, Distribution and timing of molybdenite mineralization at the El Teniente Cu-Mo porphyry deposit, Chile: Economic Geology, v. 110, p. 387–421.

Sterner, S.M., and Bodnar, R.J., 1984, Synthetic fluid inclusions in quartz: I. Compositional types synthesized and applications to experimental geochemistry: Geochimica et Cosmochimica Acta, v. 48, p. 2659-2668.

Sterner, S.M., Hall, D.L., and Bodnar, R.J., 1988, Synthetic fluid inclusions: V. Solubility relations in the system NaCI-KCl-H2O under vapor-saturated conditions: Geochimica et Cosmochimica Acta, v. 52,989-1005.

Tuttle, O.F., 1949, Two pressure vessels for silicate-water studies: Geological Society of America Bulletin, v. 60, p. 1727-1729.

van der Laan, G., Pattrick, R.A.D., Henderson, C.M.B., and Vaughan, D.J., 1992, Oxidation state variations in copper minerals studied with Cu 2*p* X-ray absorption spectroscopy: Journal of Physics and Chemistry of Solids, v. 53, p. 1185-1190.

Vry, V.H., 2010, Geological and hydrothermal fluid evolution at El Teniente, Chile: Unpublished Ph.D. thesis, London, United Kingdom, Imperial College.

Vry, V.H., Wilkinson, J. J., Seguel, J., and Millán, J., 2010, Multistage intrusion brecciation and veining at El Teniente, Chile: evolution of a nested porphyry system: Economic Geology, v. 105, p. 119-153

White, S., 1970, Ionic Diffusion in Quartz: Nature, v. 225, p. 375-376.

Zajacz, Z., and Halter, W., 2009, Copper transport by high temperature, sulfur-rich magmatic vapor: Evidence from silicate melt and vapor inclusions in a basaltic andesite from the Villarrica volcano (Chile): Earth and Planetary Science Letters, v. 282, p. 115-121.

Highlights

The controls of post-entrapment diffusion on the solubility of chalcopyrite daughter crystals in natural quartz-hosted fluid inclusions

Edward T. Spencer, Jamie J. Wilkinson, John Nolan, and Andrew J. Berry

- Quartz-hosted fluid inclusions are open with respect to H_2, H^+ and Cu^+ diffusion.
- H_2 and H^+ loss and Cu^+ gain reduce cpy solubility in natural fluid inclusions.
- Rehydrogenation of moderate salinity inclusions enables successful cpy dissolution.
- Cpy crystals in S-rich vapor inclusions fail to dissolve due to greater Cu^+ gain.
- The role of phase-separated vapors in porphyry Cu-transport is undermined.